

Thermal mass and dispersion relations of quarks in the deconfined phase of quenched QCD

Olaf Kaczmarek,^{1,*} Frithjof Karsch,^{1,2,†} Masakiyo Kitazawa,^{3,‡} and Wolfgang Söldner^{4,§}

¹*Fakultät für Physik, Universität Bielefeld, D-33615 Bielefeld, Germany*

²*Brookhaven National Laboratory, Bldg. 510A, Upton, NY 11973, USA*

³*Department of Physics, Osaka University, Toyonaka, Osaka, 560-0043, Japan*

⁴*Institut für Theoretische Physik, Universität Regensburg, D-93040 Regensburg, Germany*

(Dated: May 21, 2018)

Temporal quark correlation functions are analyzed in quenched lattice QCD for two values of temperature above the critical temperature (T_c) for deconfinement, $T = 1.5T_c$ and $3T_c$. A two-pole ansatz for the quark spectral function is used to determine the bare quark mass and the momentum dependence of excitation spectra on large lattices of size up to $128^3 \times 16$. The dependence of the quark correlator on these parameters as well as the finite volume dependence of the excitation energies are analyzed in detail in order to examine the reliability of our analysis. Our results suggest the existence of quasi-particle peaks in the quark spectrum. We furthermore find evidence that the dispersion relation of the plasmino mode has a minimum at non-zero momentum even in the non-perturbative region near T_c . We also elaborate on the enhancement of the quark correlator near the chiral limit which is observed at $T = 1.5T_c$ on about half of the gauge configurations. We attribute this to the presence of near zero-modes of the fermion matrix that are associated with non-trivial topology of the gauge configurations.

PACS numbers: 11.10.Wx, 12.38.Aw, 12.38.Gc, 14.65.-q, 25.75.Nq

I. INTRODUCTION

At asymptotically high temperature (T) strongly interacting matter, described by Quantum Chromodynamics (QCD), behaves like an almost free gas of quarks and gluons. Excitations of the medium in this temperature range are well described by dispersion relations of free quarks and gluons. As T is lowered, the temperature-dependent running coupling constant, g , increases and the excitation spectra of the elementary quark and gluon fields are modified. Eventually they deviate substantially from those of free particles. In particular at those low temperatures close but above the QCD phase transition, T_c , at which experiments at the Relativistic Heavy Ion Collider (RHIC) [1] found evidence for the existence of strong correlations in hot and dense matter, it is of interest to understand the fate of the elementary excitations, their quasi-particle properties and the structure of dispersion relations.

From leading-order resummed perturbation theory it is known that collective excitations of the quark and gluon fields acquire mass gaps (thermal masses) and decay rates proportional to gT and g^2T , respectively [2]. Since at leading order the decay rates in units of T parametrically grow faster than the thermal masses as T is lowered, it is naïvely expected that quasi-particle modes of these fields cease to exist at low temperatures at which g is large, even in the deconfined phase. On the other

hand, the experimentally observed quark number scaling of elliptic flow suggests the existence of quasi-particles having quark quantum numbers at the early stage of fireballs created in heavy ion collisions [3]. Also the behavior of quark number susceptibilities and higher-order cumulants of quark number fluctuations, calculated in lattice QCD, suggests the existence of quasi-particles even near T_c [4, 5].

One of the striking features of the quasi-particle excitations of quarks, found in leading order perturbation theory, is that the in-medium quark dispersion relation splits into two branches, the normal and plasmino modes [6]. Moreover, the latter has a non-trivial minimum at non-vanishing momentum of order gT [6]. Such a spectrum of fermions is, in fact, quite common. In the weak coupling and high T limit it is realized not only for QCD, but also in a wide class of models where the fermion couples to a boson. Away from this limiting situation the fermion spectrum has been investigated in various theoretical settings [7–16]. An interesting observation made in these studies is that the fermion spectrum exhibits a variety of structures depending on parameters of the system. For example, it has been pointed out that the fermion spectrum has a multi-peak structure when the mass of bosons that couple to the fermion is comparable with T [8]: In addition to the normal and plasmino peaks having thermal masses, there appears an additional, third dispersion which crosses the origin of the energy-momentum plane. The existence of such a multi-peak structure is also suggested in Refs. [10, 13, 16]. It is thus interesting to investigate the fate of this third branch in the quark spectrum in the non-perturbative region near but above T_c .

In order to gain insight into the quasi-particle nature of quarks in the non-perturbative region, analyses of the

* okacz@physik.uni-bielefeld.de

† karsch@bnl.gov

‡ kitazawa@phys.sci.osaka-u.ac.jp

§ wolfgang.soeldner@physik.uni-regensburg.de

spectral properties of quarks have recently been carried out on the lattice QCD [17–19]. Lattice calculations, performed in the quenched approximation of QCD in Landau gauge [17, 18] for $1.25 < T/T_c < 3.0$, indicated that a plasmino mode with a distinctively different dispersion relation contributes to the quark spectral function in addition to the normal mode even at temperatures close to T_c . In the chiral limit these modes have identical quasi-particle masses that are, in the range of temperature analyzed, approximately proportional to T . It is notable that similar results have been reported in the analysis of the quark spectrum with Schwinger-Dyson equations [12, 13].

The lattice QCD calculations presented in Refs. [17, 18], however, showed that the quasi-particle masses and dispersion relations of quarks are quite sensitive to finite volume (V) effects. The quark thermal mass drops as the aspect ratio $V^{1/3}T \equiv N_\sigma/N_\tau$ increases, and it does not converge at the value on the largest lattice in Refs. [17, 18] with $N_\sigma/N_\tau = 4$, while the lattice spacing a used in these studies was found to be fine enough to suppress lattice discretization effects. The origin of such a strong V dependence is well understood in terms of discretization effects in momentum space. For $N_\sigma/N_\tau = 4$ the lowest non-zero momentum is $p_{\min} = 2\pi(N_\tau/N_\sigma)T \simeq 1.6T$ for periodic boundary condition along the spatial direction, which is still significantly larger than T . On lattices with such an aspect ratio effects of thermally-excited particles with momenta of order T , which are responsible for the emergence of the thermal mass in terms of perturbation theory [2, 20], will thus not be properly incorporated.

In the present study, we analyze the quark correlation function on lattices with much larger aspect ratio, $N_\sigma/N_\tau = 8$. With this aspect ratio, the lowest non-zero momentum, $p_{\min} \simeq 0.79T$, is lower than T , and effects of low momentum modes are better incorporated in numerical calculations. To extract the spectral function from Euclidean lattice correlators, we use the two-pole ansatz as in the previous studies [17, 18]. We show that this ansatz reproduces the lattice correlator well on the largest lattice over rather wide ranges of bare quark masses and momenta. We use the new large volume results to improve the extrapolation of the thermal quark mass values to the infinite volume limit. We obtain a value which is about 10% smaller in magnitude than the one obtained in the earlier analysis. The large spatial volume also allows one to directly analyze the momentum dependence of excitation spectra in more detail. We show that the dispersion relation for the plasmino mode obtained with the two-pole ansatz has a minimum at non-zero momentum.

To clarify physical consequences for the quark spectral function that can be extracted from the analysis with the two-pole ansatz, we also take a closer look at the Euclidean quark correlator on the lattice. We show that with the present statistics the two-pole ansatz can give small χ^2/dof even if the quark spectral function does

T/T_c	β	N_σ	N_τ	κ_c	N_{conf}	N_{top}
3	7.457	128	16	0.133989	28	0
1.5	6.872	128	16	0.134986	101	59

TABLE I. Simulation parameters on lattices. See the text for details.

not consist solely of two peaks. Nevertheless, we argue that the analysis performed by us for finite ranges of parameters indicates the existence of quasi-particle peaks corresponding to the normal and plasmino modes having thermal masses near but above T_c .

At $T = 1.5T_c$, we find that on about half of the gauge configurations the quark correlator shows an enhancement deviating from the generic behavior near the chiral limit. We show that this behavior is sensitive to the chirality of the quark propagator and argue that it is expected to arise from gauge configurations with non-trivial topology which are still abundant at this value of the temperature. We do not find any of these effects at the larger temperature $T = 3T_c$.

This paper is organized as follows. In the next section we summarize the basic properties of the quark correlator and present our simulation setup. In Sec. III, we discuss the enhancement of the quark correlator near the chiral limit observed on some gauge configurations for $T = 1.5T_c$. In Sec. IV we analyze the dependences of the quark spectral function on the bare quark mass and momentum. The last section is devoted to a short summary. In appendix A we discuss the relation between spectral function and Euclidean correlator to clarify the sensitivity of the lattice correlator on the quark spectrum.

II. QUARK SPECTRAL FUNCTION

Excitation properties of the quark field are encoded in the quark spectral function $\rho_{\mu\nu}(\omega, \mathbf{p})$, with μ and ν denoting Dirac indices. In order to extract $\rho_{\mu\nu}(\omega, \mathbf{p})$ from lattice QCD simulations we have analyzed the quark correlator in Euclidean space

$$S_{\mu\nu}(\tau, \mathbf{p}) = \frac{1}{V} \int d^3x d^3y e^{i\mathbf{p}\cdot(\mathbf{x}-\mathbf{y})} \langle \psi_\mu(\tau, \mathbf{x}) \bar{\psi}_\nu(0, \mathbf{y}) \rangle, \quad (1)$$

on the lattice in the quenched approximation. This correlator is related to the spectral function as

$$S_{\mu\nu}(\tau, \mathbf{p}) = \int_{-\infty}^{\infty} d\omega \frac{e^{(\tau T - 1/2)\omega/T}}{e^{\omega/2T} + e^{-\omega/2T}} \rho_{\mu\nu}(\omega, \mathbf{p}). \quad (2)$$

Here, τ is the imaginary time restricted to the interval $0 \leq \tau < 1/T$, $\psi_\mu(\tau, \mathbf{x})$ is the quark operator, and V denotes the volume of the system. The quark correlator Eq. (1) has been calculated after fixing each gauge field

configuration to Landau gauge, $\partial_\mu A^\mu = 0$. In the numerical analysis, we used $(1/3)\text{tr}|\partial_\mu A^\mu|^2 < 10^{-12}$ as a stopping criterion of the gauge-fixing algorithm. The simulation parameters are summarized in Table I. We used lattices of size $N_\sigma^3 \times N_\tau = 128^3 \times 16$ for $T = 1.5T_c$ and $3T_c$. For the lattice fermion, we use non-perturbatively improved clover Wilson fermions with the clover coefficient c_{SW} taken from Ref. [18]. The number of configurations, N_{conf} , analyzed in the present study for $T = 3T_c$ is smaller than those in the previous work with $N_{\text{conf}} = 44 - 60$. With the aid of the definition of quark correlator with wall source [18], however, the statistics of the correlator improves compared to our previous analysis, as will be discussed in Sec. IV.

For $T = 1.5T_c$, we find that the quark correlators on about half of the gauge configurations show an enhancement near the chiral limit deviating from the generic behavior [21]. As described in detail in the next section, this enhancement is obviously related to the non-trivial topology of gauge field configurations. The number of configurations which are identified to be topologically non-trivial is given in Table I as N_{top} . We found that the influence of topology on the quark propagator manifest itself in the quark correlator in scalar, pseudo-scalar, and tensor channels, whereas vector and axial-vector channels are not affected. Since all analyses in this study depend only on the quark correlator in the vector channel except for the analysis of the quark mass dependence given in Fig. 5, which shows the result only for $T = 3T_c$, we have performed these analyses using all gauge configurations without distinction of topologically trivial and non-trivial ones. For $T = 3T_c$ all configurations were identified to be topologically trivial.

In the Wilson fermion formulation the quark mass, m_0 , is controlled by the hopping parameter, κ . When we discuss the m_0 dependence of the quark spectrum in what follows, we use the relation

$$m_0 = \frac{1}{a} \log \left(1 + \frac{1}{2} \left(\frac{1}{\kappa} - \frac{1}{\kappa_c} \right) \right), \quad (3)$$

which defines the pole mass of the Wilson fermion propagator. In the free case, corresponding to $\beta \rightarrow \infty$, one has $\kappa_c = 1/8$. At finite values of the gauge coupling, $\beta < \infty$, the quark mass receives an additive renormalization. In this work we determine κ_c from the behavior of the quark correlation function [18], which is presented in Table I.

III. QUARK CORRELATOR ON TOPOLOGICALLY-NONTRIVIAL CONFIGURATIONS

In the analysis of the quark correlator we found that for $T = 1.5T_c$ the correlator near the chiral limit shows a large enhancement deviating from the generic behavior [18] on about half the gauge configurations analyzed in this study. At $T = 3T_c$, on the other hand, no such effect has been observed.

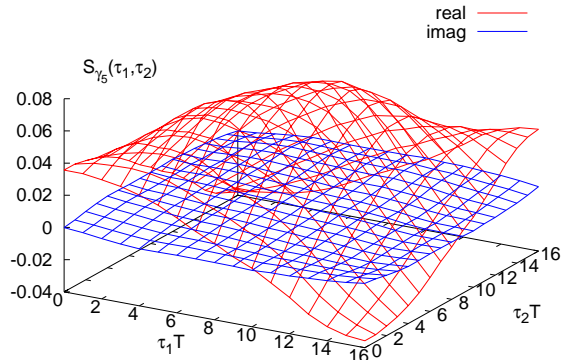


FIG. 1. Real and imaginary parts of quark correlator in the pseudo-scalar channel, $S_{\gamma_5}(\tau_1, \tau_2)$, on a topologically-nontrivial gauge configuration for $T = 1.5T_c$.

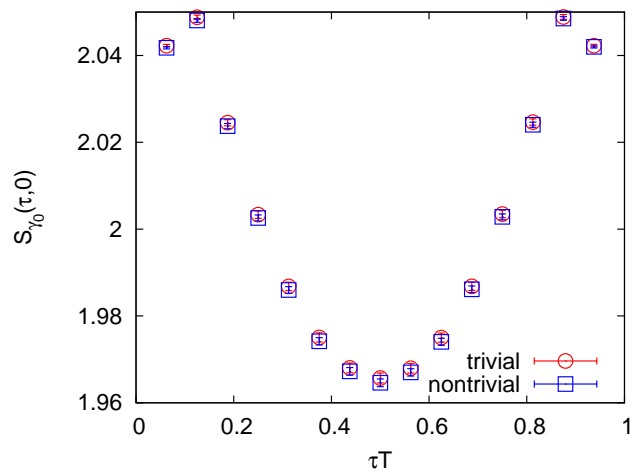


FIG. 2. Quark correlators in the temporal component of vector channel, $S_{\gamma_0}(\tau)$, averaged over topologically trivial and non-trivial gauge configurations for $T = 1.5T_c$.

In this section, we summarize the behavior of the quark correlator on these configurations. We show that characteristic features of this enhancement of the quark correlator are consistent with expectations for the behavior of a quark propagator on gauge field configurations with non-trivial topology which give rise to zero modes of the Dirac operator with definite chirality [22].

The Dirac structure of the quark correlator for $\mathbf{p} = 0$ is decomposed into its different quantum number channels

$$S_\Gamma(\tau_1, \tau_2) = \frac{1}{4V} \int d^3x d^3y \text{Tr}_D [\Gamma \langle \psi(\tau_1, \mathbf{x}) \bar{\psi}(\tau_2, \mathbf{y}) \rangle], \quad (4)$$

where Tr_D denotes the trace over Dirac indices with $\Gamma = 1, \gamma_5, \gamma_\mu, \gamma_\mu \gamma_5$, and $i[\gamma_\mu, \gamma_\nu]/2$ for scalar, pseudo-

total	N_0	N_L	N_R	N_{LR}
101	42	14	40	5

TABLE II. Number of configuration for $T = 1.5T_c$ having no anomalous behavior (N_0), having in left- and right-handed channels (N_L and N_R , respectively), and in both channels (N_{LR}).

scalar, vector, axial-vector, and tensor channels, respectively. In Fig. 1 we show the quark correlator in the pseudo-scalar channel, $S_{\gamma_5}(\tau_1, \tau_2)$, in the vicinity of the chiral limit on a configuration which is identified to be topologically non-trivial. The quark correlator in the pseudo-scalar channel should vanish when the system is invariant under parity transformation. In fact, on all configurations for $T = 3T_c$, we have checked that $S_{\gamma_5}(\tau_1, \tau_2)$ is negligibly small compared to scalar and vector channels. For $T = 1.5T_c$, however, on about half of the configurations $S_{\gamma_5}(\tau_1, \tau_2)$ shows an enhancement as in Fig. 1 near the chiral limit. The amplitude of this behavior rises with increasing κ , i.e., decreasing quark mass, and takes the largest value for κ near the critical value κ_c , at which the sign is flipped. A similar behavior is observed in scalar and tensor channels on these configurations. On the other hand, such an enhancement does not appear in vector and axial-vector channels. As an example, in Fig. 2 we show the temporal component of the quark correlators in the vector channel with $\mathbf{p} = 0$, $S_{\gamma_0}(\tau, 0)$, in the vicinity of the chiral limit averaged separately over topologically trivial and non-trivial configurations for $T = 1.5T_c$. The figure shows that the vector-channel correlator on each set of configurations does not give a statistically-significant difference.

Our numerical result also shows that on many configurations which are identified to be topologically non-trivial the enhancement manifests itself only on either the left- or right-handed correlator, which are defined as

$$S_{L,R}(\tau, \mathbf{p}) = \frac{1}{2} \text{Tr}_D[\Lambda_{\pm} S(\tau, \mathbf{p})], \quad (5)$$

with projection operators onto left- and right-handed quarks, $\Lambda_{\pm} = (1 \pm \gamma_5)/2$. In Table II, we show the number of configurations having the enhancement in the left- and right-handed channels (N_L and N_R), respectively, and without the enhancement (N_0). On some configurations an enhancement of the correlator is observed both in left- and right-handed channels. Their number is denoted by N_{LR} and is also given in Table II.

These results on the enhancement of the quark correlator near the chiral limit strongly indicate that they are related to a zero mode of the Dirac operator which, for instance, may be associated with the presence of instantons on these configurations. Using the eigenvalues and eigenmodes of the Dirac operator $D = \gamma_{\mu}(\partial_{\mu} + igA_{\mu})$,

$$D\psi_{\lambda}(x) = \lambda\psi_{\lambda}(x), \quad (6)$$

the quark propagator, which is the inverse of $iD + m$, is written as

$$S(x, y) = \sum_{\lambda} \frac{1}{i\lambda + m} \psi_{\lambda}(x) \psi_{\lambda}^{\dagger}(y), \quad (7)$$

where x and y represent positions in Euclidean space. On a gauge field configuration having an instanton, the Dirac operator has a zero mode ψ_0 [22], and the quark propagator is decomposed as

$$\begin{aligned} S(x, y) &= \frac{1}{m} \psi_0(x) \psi_0^{\dagger}(y) + \sum_{\lambda \neq 0} \frac{1}{i\lambda + m} \psi_{\lambda}(x) \psi_{\lambda}^{\dagger}(y) \\ &\equiv S_I(x, y) + S_{\lambda}(x, y), \end{aligned} \quad (8)$$

with

$$S_I(x, y) = \frac{1}{m} \psi_0(x) \psi_0^{\dagger}(y). \quad (9)$$

The zero mode associated with an instanton belongs to the left-handed spinor and satisfies $\Lambda_+ \psi_0 = \psi_0$. Accordingly, S_I satisfies

$$S_I(x, y) = \Lambda_+ S_I(x, y) \Lambda_+. \quad (10)$$

On a configuration having an anti-instanton, the zero mode is right-handed, $\Lambda_- \psi_0 = \psi_0$, and Λ_+ in Eq. (10) are replaced with Λ_- . Eq. (10) shows that the zero mode cannot affect vector and axial-vector channels, since in these channels Γ in Eq. (4) contains one gamma matrix, and hence $\text{Tr}_D[\Gamma \Lambda_{\pm}] = 0$.

All these properties of S_I agree with the behavior of the quark correlator observed on the lattice for $T = 1.5T_c$ discussed above. Gauge configurations in N_L and N_R would have one or more instantons and anti-instantons, respectively, and those in N_{LR} have both an instanton and an anti-instanton. We have also checked that the quark correlator near the chiral limit on topologically non-trivial configurations approximately satisfies

$$S_{\Gamma}(\tau_1, \tau_2) = [S_{\Gamma}(\tau_2, \tau_1)]^*, \quad (11)$$

for pseudo-scalar and tensor channels (an example is given in Fig. 1), which is consistent with Eq. (9).

Assuming that the enhancement of the quark correlator indeed arises from configurations with non-zero topological charge one can estimate the topological susceptibility at that value of the temperature

$$\chi_Q = \frac{T \langle \delta Q^2 \rangle}{V}, \quad (12)$$

where $Q = n_+ - n_-$ is the topological charge with n_{\pm} being the numbers of instantons and anti-instantons, respectively, and VT^{-1} is the four-volume in Euclidean space. Provided that each configuration in N_L and N_R contains only one instanton and anti-instanton, respectively, and $Q = 0$ on configurations in N_{LR} , one obtains $\langle \delta Q^2 \rangle = (N_L + N_R)/N_{\text{conf}} \simeq 0.53$ for $T = 1.5T_c$. Using

this result in Eq. (12) with $VT^3 = 8^3$ we obtain an estimate for the topological susceptibility of $\chi_Q^{1/4} \simeq 0.11T$ for this temperature. We emphasize that this is a rough estimate since the value of $\langle \delta Q^2 \rangle$ alters if some topologically non-trivial configurations have more than one (anti-)instanton. Moreover, while the separation between gauge configurations is a few times larger than the auto-correlation length measured in terms of the plaquette and Polyakov loop correlation functions [21], this may not be the case for topology and the gauge configurations may not be separated well enough in Monte Carlo time to suppress a long auto-correlation of Q . It is, however, notable that the value of χ_Q estimated here seems to agree with the previous study of χ_Q on quenched lattice for non-zero T [23].

The influence of non-trivial topological structures on the quark correlator is expected to be non-vanishing also in the thermodynamic limit on the quenched lattice. First, we have numerically checked that the effect does not cancel out on a single configuration when averaging correlation functions over the temporal direction,

$$\bar{S}(\tau) = \frac{1}{N_\tau} \sum_{\tau'} S(\tau + \tau', \tau'). \quad (13)$$

Second, the numbers of (anti-)instantons, n_\pm , increase proportional to V , while $\langle |\delta Q| \rangle$ is proportional to $V^{1/2}$ [24]. This insures that the topological susceptibility is well defined in the thermodynamic limit. Third, instantons and anti-instantons affect different channels in the quark correlator, respectively, and the numerical result indicates that their effect has a definite sign in each channel. Therefore, effects of topology do not cancel out by their average in the thermodynamic limit. The non-trivial topological properties of the quark propagator observed here thus will give rise to physical contributions in various observables, such as those observed as $U(1)_A$ anomaly.

Although the non-trivial topology of gauge configurations gives rise to non-vanishing contributions to the quark correlator, our numerical result for $T = 1.5T_c$ shows that the quark propagators in the vector and axial-vector channels are not affected by this effect as shown in Fig. 2. Since all analyses in Sec. IV and appendix A rely only on the vector channel, except for the one for Fig. 5, we use all gauge configurations including topologically trivial and non-trivial ones in these analyses. From the insensitivity of the vector and axial-vector channel correlators on topology, it is anticipated that the instanton distribution for $T = 1.5T_c$ is sufficiently dilute so that each instanton affects the quark propagator as S_1 in Eq. (8) almost independently [24]. The analysis on the thermal mass and the dispersion relation performed in Sec. IV would then be interpreted as the one for the remaining part S_λ .

The discussion on the relation between the topology of gauge configurations and the enhancement of the quark correlator given in this section clearly addresses an im-

portant aspect of QCD thermodynamics and requires further analysis. We intend to explore the interplay of topology, zero modes, eigenfunctions and the structure of the quark propagator in a forthcoming publication [25].

IV. QUARK EXCITATION SPECTRA

A. Quark spectral function and two-pole ansatz

The Dirac structure of the quark spectral function $\rho_{\mu\nu}(\omega, \mathbf{p})$ at finite temperature is decomposed as

$$\begin{aligned} \rho_{\mu\nu}(\omega, \mathbf{p}) \\ = \rho_0(\omega, p)(\gamma^0)_{\mu\nu} - \rho_v(\omega, p)(\hat{\mathbf{p}} \cdot \boldsymbol{\gamma})_{\mu\nu} + \rho_s(\omega, p)\mathbf{1}_{\mu\nu}, \end{aligned} \quad (14)$$

where $p = |\mathbf{p}|$ and $\hat{\mathbf{p}} = \mathbf{p}/p$ [2]. In this section we consider the spectral function above T_c for two cases; (1) for zero momentum, and (2) in the chiral limit [18]. With $p = 0$, $\rho_v(\omega, p)$ vanishes in Eq. (14) and $\rho_{\mu\nu}(\omega, \mathbf{p} = \mathbf{0})$ is decomposed with the projection operators $L_\pm = (1 \pm \gamma^0)/2$ as

$$\rho(\omega, \mathbf{0}) = \rho_+^M(\omega)L_+\gamma^0 + \rho_-^M(\omega)L_-\gamma^0, \quad (15)$$

with

$$\rho_\pm^M(\omega) = \frac{1}{2} \text{Tr}_D [\rho(\omega, \mathbf{0})\gamma^0 L_\pm]. \quad (16)$$

In the chiral limit and for $T > T_c$, the system possesses the chiral symmetry and $\rho_s(\omega, p)$ vanishes. $\rho_{\mu\nu}(\omega, \mathbf{p})$ is then decomposed with the projection operators $P_\pm(\mathbf{p}) = (1 \pm \gamma^0 \hat{\mathbf{p}} \cdot \boldsymbol{\gamma})/2$ as

$$\rho(\omega, \mathbf{p}) = \rho_+^P(\omega, p)P_+(\mathbf{p})\gamma^0 + \rho_-^P(\omega, p)P_-(\mathbf{p})\gamma^0, \quad (17)$$

with

$$\rho_\pm^P(\omega, p) = \frac{1}{2} \text{Tr}_D [\rho(\omega, \mathbf{p})\gamma^0 P_\pm(\mathbf{p})]. \quad (18)$$

Using the charge conjugation symmetry one can show that

$$\rho_\pm^M(\omega) = \rho_\mp^M(-\omega), \quad \rho_\pm^P(\omega, p) = \rho_\mp^P(-\omega, p). \quad (19)$$

In the chiral limit and for $p = 0$, both $\rho_s(\omega, p)$ and $\rho_v(\omega, p)$ vanish and one obtains

$$\rho_\pm^M(\omega) = \rho_\pm^P(\omega, 0) = \rho_0(\omega, 0). \quad (20)$$

In order to extract the quark spectral function from lattice correlator, we follow the approach taken in Refs. [17, 18], which makes use of a two-pole ansatz for the spectrum,

$$\rho_\pm^{M,P}(\omega) = Z_1\delta(\omega - E_1) + Z_2\delta(\omega + E_2). \quad (21)$$

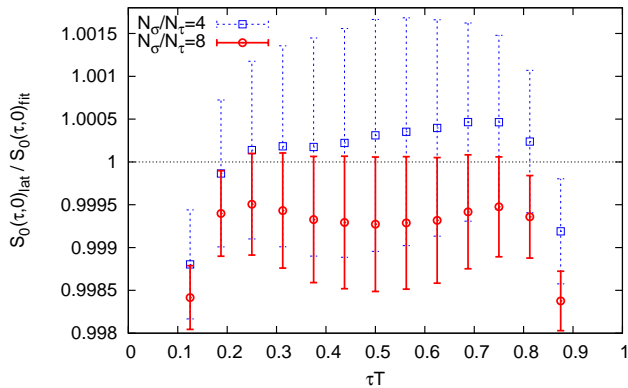


FIG. 3. Lattice correlator $S_0(\tau)_{\text{lat}}$ in the chiral limit normalized by the fitting function Eq. (22) for $T/T_c = 3$. Solid and dashed lines represent the results for $N_\sigma/N_\tau = 8$ and 4, respectively.

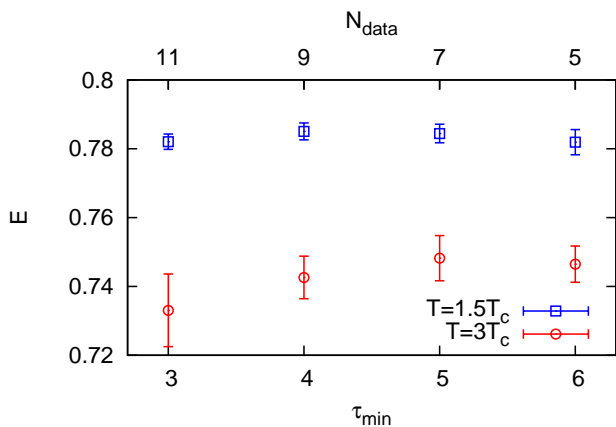


FIG. 4. τ_{min} dependence of fitting parameter E in the fit with Eq. (22) to $S_0(\tau, \mathbf{0})_{\text{lat}}$ in the chiral limit.

Here, $Z_{1,2}$, and $E_{1,2} > 0$, are fitting parameters that will be determined from correlated fits to the lattice correlator: $Z_{1,2}$ and $E_{1,2}$ represent the residues and positions of poles, respectively. By comparing the fit results with spectral functions obtained in perturbative calculations one can identify the pole at $\omega = E_1$ to be the normal mode, while the one at $\omega = -E_2$ corresponds to the plasmino mode [7, 8, 18]. To determine the fit parameters with correlated fits, we use lattice data points at $\tau_{\text{min}} \leq \tau/a \leq N_\tau - \tau_{\text{min}}$ with the number of points $N_{\text{data}} = N_\tau - 2\tau_{\text{min}} + 1$.

Before discussing the analysis of the quark spectrum with this fitting function, let us examine the behavior of the quark correlator, Eq. (1), on the lattice and discuss how the fitting function Eq. (21) reproduces it. To simplify the argument we limit our attention for the moment to the case in the chiral limit with $p = 0$. The Dirac structure of the spectral function is then proportional to

γ^0 , $\rho(\omega, \mathbf{0}) = \rho_0(\omega, 0)\gamma^0$, and the Euclidean correlator is solely given by the one corresponding to this channel, $S_0(\tau, 0) = \text{Tr}_D[S(\tau, \mathbf{0})\gamma_0]$. Since $\rho_0(\omega, 0)$ is even in ω , the ansatz Eq. (21) reduces to

$$\begin{aligned} \rho_0(\omega, 0) &= \rho_+^M(\omega) = \rho_+^P(\omega, 0) \\ &= Z(\delta(\omega - E) + \delta(\omega + E)), \end{aligned} \quad (22)$$

which involves only two fit parameters, Z and E . In Fig. 3 we show the lattice correlator $S_0(\tau, 0)_{\text{lat}}$ for $T/T_c = 3$ normalized by the one constructed from the fitting function Eq. (22), $S_0(\tau, 0)_{\text{fit}}$, with fitting parameters determined from a correlated fit with $\tau_{\text{min}} = 4$. The figure shows that the fit result, $S_0(\tau, 0)_{\text{fit}}$, well reproduces the lattice results, $S_0(\tau, 0)_{\text{lat}}$, for $\tau T \simeq 0.5$. We have checked that the fitting parameters do not have a statistically significant dependence on the choice of τ_{min} for $3 \leq \tau_{\text{min}} \leq 6$. This is evident from the dependence of E on τ_{min} . Results obtained in the chiral limit are shown in Fig. 4. In Fig. 3, clear deviations between $S_0(\tau, 0)_{\text{fit}}$ and $S_0(\tau, 0)_{\text{lat}}$ are observed for small and large τ , which can be attributed to distortion effects arising from the source [18, 26]. For $\tau_{\text{min}} \leq 2$, χ^2/dof of the fit becomes unacceptably large due to the distortion effect. Similar results are obtained for all parameters analyzed in this study with Eq. (21). In the following, we use $\tau_{\text{min}} = 4$, which is chosen in order to reduce the distortion effect and at the same time leave us with a sufficient number of data points for our four parameter fits. We found that with $\tau_{\text{min}} = 4$ fits with the pole ansatz give reasonable values of chi-square, $0.5 < \chi^2/\text{dof} < 3$, for $m_0/T \lesssim 0.5$ and $p/T \lesssim 3$.

We remark that, although the two-pole ansatz Eq. (21) reproduces the lattice correlator quite well with a small χ^2/dof , this result does not necessarily mean that the quark spectral function is solely composed of two sharp peaks at energies $\omega = E_1$ and $-E_2$. In fact, as discussed in appendix A, the Euclidean correlator is insensitive to the structure of the spectral function at $|\omega| \lesssim T$. Although with our current statistics the quark propagator at all distances is determined to better than 0.1%, the spectrum in this low energy range generally still suffers from large uncertainties. In Sec. IV C and appendix A, we will discuss how our analysis of the quark spectrum is influenced by this problem. Nevertheless, we will assert in these sections that, from the success of the two-pole ansatz over wide ranges of m_0 and p , it is reasonable to expect that the quark spectrum contains peak structures corresponding to the normal and plasmino modes. Qualitative dependences of the positions of these peaks on m_0 and p are then analyzed with the fitting parameters E_1 and E_2 .

Finally, we briefly comment on the statistical errors of the quark correlator in this analysis. In Fig. 3, the quark correlator obtained in Ref. [18] with $N_\sigma/N_\tau = 4$ for $T = 3T_c$ is shown by the dotted lines together with the present result with $N_\sigma/N_\tau = 8$. The figure shows that the error-bars for $N_\sigma/N_\tau = 8$ is about 40% smaller in magnitude than that for $N_\sigma/N_\tau = 4$, although the

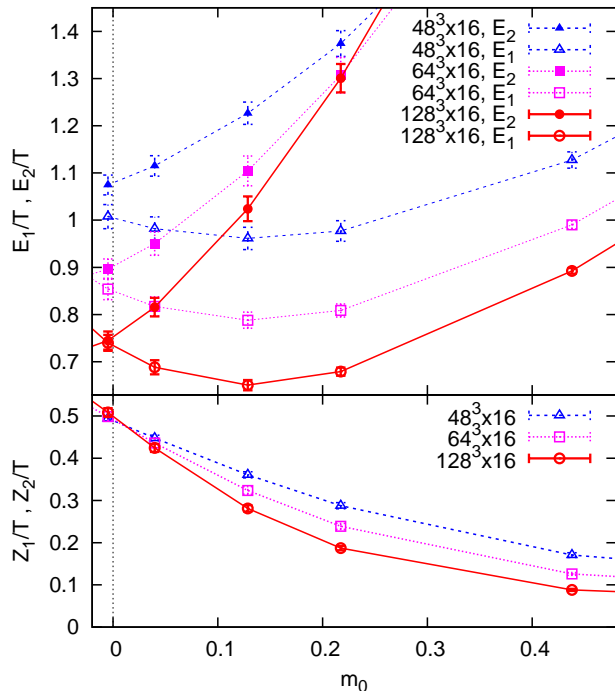


FIG. 5. Bare quark mass dependence of parameters E_1 , E_2 at $T = 3T_c$ on lattices with $N_\sigma/N_\tau = 8, 4$ and 3 .

N_σ/N_τ	3	4	8	∞
$T/T_c = 3$	1.041(16)	0.875(8)	0.743(6)	0.725(14)
$T/T_c = 1.5$	1.075(14)	0.906(8)	0.784(3)	0.768(11)

TABLE III. The values of m_T/T obtained on lattices with $N_\sigma/N_\tau = 3, 4$ and 8 . The far right column shows the values of m_T estimated by the extrapolation to the infinite volume limit.

former result is obtained with only about half as many configurations than the latter ($N_{\text{conf}} = 51$). As mentioned previously, this improvement in statistics is a consequence of the use of the wall source in the numerical analysis of quark correlators [18]. We have checked that the distribution of correlators obtained on each gauge configuration around the average is approximately proportional to $V^{-1/2}$. Such a scaling with the wall source is to be expected when the spatial extent of the lattice, L , is larger than the coherence length of the quark field, ξ . Estimating $\xi T \simeq T/m_T \simeq 1.25$ and $LT = N_\sigma/N_\tau = 8$ this, indeed, seems to hold.

B. Excitation spectra for $p = 0$

In this subsection, we focus on the quark spectrum with $p = 0$, which is decomposed into $\rho_\pm^M(\omega)$ as in Eq. (15), and analyze the m_0 dependence of the spec-

trum. In Fig. 5, we show results for the m_0 dependence of fitting parameters, E_1 , E_2 , and $Z_2/(Z_1 + Z_2)$ for $T = 3T_c$. We compare the results on lattices with smaller aspect ratios $N_\sigma/N_\tau = 3$ (triangles) and 4 (squares) [17, 18] with our new results on the $128^3 \times 16$ lattice (circles). One sees that the qualitative behavior of fitting parameters on the largest lattice agrees with previous results obtained on lattices with smaller N_σ/N_τ . The ratio $Z_2/(Z_1 + Z_2)$ becomes larger as m_0 is decreased, and eventually reaches $Z_2/(Z_1 + Z_2) = 0.5$ in the chiral limit. At this point, which defines κ_c in Eq. (3), $E_1 = E_2$ is satisfied within the statistical error. The thermal mass is defined as $m_T \equiv (E_1 + E_2)/2$ on this point, or equivalently $m_T \equiv E$ with the fit with Eq. (22) to $S_0(\tau, 0)$. For $m_0 > 0$, E_1 has a minimum, while E_2 is a monotonically increasing function. For $T = 1.5T_c$, the same analysis can be performed on topologically trivial gauge configurations, which gives qualitatively the same result as in Fig. 5.

Figure 5 also shows that the values of E_1 and E_2 drop significantly with increasing aspect ratio N_σ/N_τ . Accordingly, the value of m_T also has a strong N_σ/N_τ dependence. The value of m_T/T for $N_\sigma/N_\tau = 3, 4$ and 8 for $T/T_c = 1.5$ and 3 is given in Table III. To infer the thermal mass in the infinite volume limit, we performed an extrapolation of m_T to infinite volume with an ansatz

$$m_T(1/V) \sim m_T(0) \exp(c/V) \quad (23)$$

using the results with $N_\sigma/N_\tau = 4$ and 8 . The result of this extrapolation is shown in the far right column of Table III. The infinite volume extrapolated values of m_T for each T obtained in this study is about 10% smaller in magnitude than those estimated in Ref. [18]. It is also notable that the ratio m_T/T increases as T is lowered, which was not observed in the previous study [18]. With the present extrapolation, the value of m_T in the infinite volume limit coincides with the one obtained for $N_\sigma/N_\tau = 8$ within the statistical error. This result suggests that the influence of finite volume effects on m_T is well suppressed for $N_\sigma/N_\tau = 8$.

In Fig. 5, one also finds that the value of κ_c , *i.e.* m_0 at which $Z_2/(Z_1 + Z_2) = 0.5$, slightly shifts with the variation of N_σ/N_τ . The difference of κ_c between the two largest lattices $N_\sigma/N_\tau = 4$ and 8 , however, is within the statistical error.

C. Dispersion relations at non-zero p

Next, we set $\kappa = \kappa_c$ and analyze the momentum dependence of the excitation spectra at non-zero momentum in the chiral limit using the decomposition in Eq. (17). For the analysis of the quark correlator at non-zero p for $T = 1.5T_c$, we have performed the analysis on 54 configurations including topologically trivial and non-trivial ones. In Fig. 6 we show the momentum dependence of E_1 and E_2 normalized by m_T , as well as $Z_2/(Z_1 + Z_2)$, for $T/T_c = 1.5$ and 3 . The horizontal axis represents the momentum of a free fermion on the lattice, $\hat{p} = (1/a) \sin pa$,

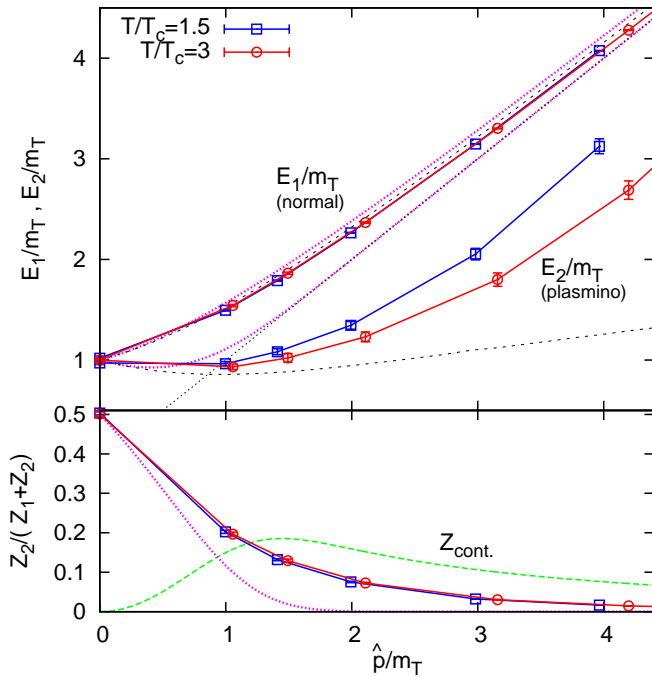


FIG. 6. Dependences of the fitting parameters E_1 and E_2 and the ratio $Z_2/(Z_1 + Z_2)$ on the lattice momentum $\hat{p} = (1/a)\sin(pa)$ for $T/T_c = 1.5$ and 3. See, the text for the explanation of other lines.

normalized by m_T . The figure shows that the qualitative features of the dispersion relations as functions of \hat{p} do not change compared to our earlier results on lattices with smaller aspect ratio [18]: $E_1 > E_2$ is always satisfied in contrast with the results in the previous subsection, and E_2 enters the space-like region at high momentum. We note that a similar result is obtained from the analysis of the quark spectrum in the Schwinger-Dyson approach [12, 13]. The decrease of $Z_2/(Z_1 + Z_2)$ for large momentum shows that the plasmino mode ceases to exist as p becomes larger.

At asymptotically high temperatures the quark spectrum is calculated perturbatively [2, 20]. The dispersion relations of the normal and plasmino modes obtained at the one-loop order are shown in Fig. 6 by the dotted lines with $m_T = gT/\sqrt{6}$. The residue of the plasmino mode in the normalization of the quark field $\int_{-\infty}^{\infty} d\omega \rho_+^P(\omega, p) = 1$ is also shown in the lower panel by the dotted line. Besides these poles, $\rho_+^P(\omega, p)$ at the one-loop order has a continuum in the space-like region. The spectral weight of the continuum, $Z_{\text{cont}} \equiv \int_{-p}^p d\omega \rho_+^P(\omega, p)$, is shown in the lower panel by the dashed line, which in the perturbative analysis reaches at most exceeds $Z_{\text{cont}} \simeq 0.18$.

The numerical result for E_2 presented in Fig. 6 shows that the result for the lowest non-zero momentum, $p_{\text{min}} = 2\pi(N_\tau/N_\sigma)T$, is significantly lower than m_T ; *i. e.* $m_T/T \simeq E_2/T|_{p=0} = 0.742(12)$ and $E_2/T|_{p=p_{\text{min}}} = 0.694(21)$ for $T/T_c = 3$ and $E_2/T|_{p=0} = 0.782(9)$ and

$E_2/T|_{p=p_{\text{min}}} = 0.758(18)$ for $T/T_c = 1.5$. Provided that the value of E_2 in our two-pole ansatz represents the dispersion relation of the plasmino mode, this result serves as direct evidence for the existence of the plasmino minimum in the non-perturbative analysis. One, however, has to be careful with this interpretation. As we have argued previously and in appendix A, the Euclidean correlator is insensitive to the spectral function at low energy, $|\omega| \lesssim T$, and analysis of the spectrum in this energy range has large uncertainty. In fact, in terms of the comparison with the perturbative result our fitting function does not contain the continuum in the space-like region.

In order to see the effect of the continuum part in the spectral function at the one-loop order on the Euclidean correlator, we have performed the following analysis. First, we calculated the Euclidean correlator at one-loop order in perturbation theory, $S_{\text{HTL}}(\tau, \mathbf{p})$. We then performed the two-pole fit with Eq. (21) to discrete points of $S_{\text{HTL}}(\tau, \mathbf{p})$ with the same discretization as on the lattice. To estimate the chi-square of the fit, we put error-bars and Gaussian noise on each value of $S_{\text{HTL}}(\tau, \mathbf{p})$ following the covariance matrix obtained on the lattice. With this analysis, we found that the two-pole fit to $S_{\text{HTL}}(\tau, \mathbf{p})$ gives a reasonable chi-square, $\chi^2/\text{dof} \simeq 1$, although the spectral function corresponding to $S_{\text{HTL}}(\tau, \mathbf{p})$ contains the continuum. The values of E_1 and E_2 obtained by the fit to $S_{\text{HTL}}(\tau, \mathbf{p})$ are shown by the dashed lines in the upper panel of Fig. 6. One sees that these results considerably deviate from the positions of normal and plasmino modes. In particular, we note that E_2 also enters the space-like region for $p \gtrsim T$. This result obviously shows that the success of the pole ansatz does not mean the absence of the continuum. The values of E_1 and E_2 thus should not be regarded as the positions of peaks, but a center of spectral weights in some sense in the positive and negative energy regions. It also suggests that in our current analysis the normal mode is quantitatively much better under control than the plasmino branch.

Nonetheless, some qualitative features on the quark spectrum can be extracted from our results. First, as discussed in Appendix A, the consistent success of the two-pole ansatz over wide parameter ranges suggests that the quark spectrum has peak structures at positive and negative energies in the range of m_0 and p analyzed in this study. Next, the momentum dependences of the peak positions in $\rho_+^P(\omega, p)$ can be constrained by general properties of the spectral function. Using the relation Eq. (19) and the analyticity of $\rho(\omega, \mathbf{p})$, one can show that (1) if $\rho_+^P(\omega, p)$ at $p = 0$ has a peak at positive energy $\omega = E_+^*(0)$, there also exists a peak at negative energy with the same absolute value, $\omega = -E_-^*(0) = -E_+^*(0)$, and (2) momentum dependences of the peak positions $\omega = E_+^*(p)$ and $-E_-^*(p)$ satisfy $dE_+^*/dp = -dE_-^*/dp$ at $p = 0$.¹ The result in Fig. 6 indicates not only a nega-

¹ A discussion of a similar relation for position of *poles* in the

tive dE_2/dp at $p = 0$ but also a positive dE_1/dp . It thus seems reasonable to conclude that the dispersion relation of the plasmino peak, $E_-^*(p)$, has a negative derivative near $p = 0$. This result then leads to the existence of a minimum of $E_-^*(p)$, provided that the plasmino peak survives at sufficiently high momentum where the dE_-^*/dp becomes positive.

V. BRIEF SUMMARY

In this study, we extended the analysis of the quark spectral function on quenched lattices, performed in previous work [17, 18], to lattices with larger spatial volume. With this analysis we achieved considerable progress in the understanding of finite spatial volume effects on the quark correlator and confirmed the importance of non-trivial topological configurations for the structure of the quark propagator at temperatures above T_c . The strong V dependence observed in a previous study with aspect ratios $N_\sigma/N_\tau = 3$ and 4 seems to converge on the largest lattice with $N_\sigma/N_\tau = 8$. An extrapolation of the quark thermal mass, m_T , to the infinite volume is about 10% smaller than the earlier estimate [18].

Dependences of the fitting parameters in the two-pole ansatz on m_0 and p do not change qualitatively on the largest lattice. We, however, found that the position of the pole corresponding to the plasmino, E_2 , has a minimum at non-zero momentum within the ansatz. As discussed in Sec. IV C, this result with the pole ansatz does not directly mean the existence of the minimum of the plasmino dispersion (See also, Ref. [12]). The quark correlator obtained on the lattice as functions of continuous parameters m_0 and p , however, strongly indicates the existence of the plasmino peaks and that the dispersion relation of the plasmino has a negative slope at low momentum near T_c .

We also presented evidence for the influence of non-trivial topology of gauge field configurations on the structure of the quark propagator. This clearly is visible in our data at $T = 1.5T_c$, while at $T = 3T_c$ we do not observe topologically non-trivial configurations. We showed that, nonetheless, the vector and axial vector channels are not influenced by this effect at $T = 1.5T_c$. We expect that the effect of non-trivial topology will modify the structure of the quark propagator in the quenched QCD significantly as T approaches T_c from above. The analysis of correlators near T_c therefore requires a careful treatment of this effect.

quark spectral function is presented in [27] The extension of this argument to the position of *peaks* is straightforward. This feature is graphically seen, for example, in the contour maps of spectral functions in Ref. [8].

Appendix A: Difficulty in analyzing the low energy structure of spectral functions

In this study, we have used the two-pole ansatz Eq. (21) to examine the quark spectrum from Euclidean lattice correlator. This ansatz is found to reproduce the lattice correlator well over wide parameter ranges. In this appendix, we address the significance of the success of the two-pole ansatz. We show that this success to some extent is due to a poor resolution of the lattice correlator on the spectral function at low energy, $|\omega| \lesssim T$. The insensitivity of the Euclidean correlator to low-energy spectrum has been recognized through the studies of spectral functions on the lattice, especially efforts to extract transport properties [28–30]. Since the spectral weight of quarks with a small mass and a momentum concentrates in the energy range $|\omega| \lesssim T$, our analysis suffers from the same difficulty.

In the next subsection we first summarize the problem of the insensitivity in terms of the power series expansion of correlators. We then take a closer look at the quark correlator in Sec. A 2.

1. Moment expansion

Let us consider a Euclidean correlator $S(\tau)$ and a spectral function $\rho(\omega)$ which are related to each other as

$$S(\tau) = \int_{-\infty}^{\infty} d\omega \frac{e^{(\tau T - 1/2)\omega/T}}{e^{\omega/2T} + \zeta e^{-\omega/2T}} \rho(\omega), \quad (\text{A1})$$

where $\zeta = \pm 1$ for fermions and bosons, respectively. By Taylor expanding $\exp[(\tau T - 1/2)\omega/T]$, Eq. (A1) is written as

$$S(\tau) = \sum_n C_n \left(\tau T - \frac{1}{2} \right)^n, \quad (\text{A2})$$

where the coefficients C_n are given by the moments of thermal spectral function, $\rho'(\omega) \equiv \rho(\omega)/(e^{\omega/2T} + \zeta e^{-\omega/2T})$,

$$C_n = \frac{1}{n!} \int_{-\infty}^{\infty} d\omega \left(\frac{\omega}{T} \right)^n \rho'(\omega, p). \quad (\text{A3})$$

One can show that the power series Eq. (A2) converges for $0 < \tau < 1/T$ for spectral functions having an asymptotic form $\rho(\omega) \sim \zeta \omega^m$ for large $|\omega|$.

In lattice simulations one obtains the values of $S(\tau)$ for N_τ discrete τ values with statistical errors. Through Eq. (A1), these values of $S(\tau)$ provide N_τ 'pieces of different' information on the structure of $\rho(\omega)$. The coefficients of the power series, C_n , can be interpreted as the different representation of this information.

To consider how the information of low-energy structure of $\rho(\omega)$ is encoded in $S(\tau)$, we decompose $\rho(\omega)$ into low and high energy parts as $\rho(\omega) = \rho_\Lambda(\omega) + \rho_{\text{high}}(\omega)$ with $\rho_\Lambda(\omega) = \rho(\omega)\theta(\Lambda - |\omega|)$ with some energy Λ . Since

$S(\tau)$ and $\rho(\omega)$ are related with each other linearly, one can then also decompose $S(\tau)$ into contributions of low and high energy spectrum. The contribution of $\rho_\Lambda(\omega)$ is written as

$$S_\Lambda(\tau) \equiv \int d\omega \frac{e^{(\tau T - 1/2)\omega/T}}{e^{\omega/2T} + \zeta e^{-\omega/2T}} \rho_\Lambda(\omega) = \sum_n S_n^{(\Lambda)}(\tau), \quad (\text{A4})$$

with

$$S_n^{(\Lambda)}(\tau) = C_n^{(\Lambda)} \left(\tau T - \frac{1}{2} \right)^n, \quad (\text{A5})$$

$$C_n^{(\Lambda)} = \frac{1}{n!} \int_{-\Lambda}^{\Lambda} d\omega \left(\frac{\omega}{T} \right)^n \rho'(\omega). \quad (\text{A6})$$

To avoid unnecessary complexity in the following we limit our attention to the spectral function satisfying $\rho(\omega) = \zeta \rho(-\omega) \geq 0$ for $\omega > 0$. Odd terms in Eq. (A6) then vanish while $C_n^{(\Lambda)} \geq 0$ for even n . With the aid of inequalities $(\omega/T)^n \leq (\Lambda/T)^n$ in the integrand of Eq. (A6) and $|\tau T - 1/2| < 1/2$, one then obtains an inequality

$$\frac{S_n^{(\Lambda)}(\tau)}{S(\tau)} \leq \frac{S_n^{(\Lambda)}(\tau)}{S_0^{(\Lambda)}(\tau)} \leq \frac{1}{n!} \left(\frac{\Lambda}{2T} \right)^n. \quad (\text{A7})$$

This inequality provides an upper limit of the contribution of $S_n^{(\Lambda)}(\tau)$ to $S(\tau)$, *i.e.* the relative strength of signals for information on each moment of $\rho'_\Lambda(\omega)$ encoded in $S(\tau)$. Eq. (A7) tells us that if we choose $\Lambda \lesssim T$ the contribution of higher order moments is strongly suppressed due to the factorial and exponential factors. The decrease of the signals makes evaluations of their values difficult. In practical analyses with statistical errors, therefore, the number of moments, *i.e.* the number of independent information on $\rho_\Lambda(\omega)$, which can be estimated from the correlator is severely limited with Eq. (A7). For example, if one wants to examine $\rho_\Lambda(\omega)$ with $\Lambda = T$ from the lattice correlator having statistical errors of order 0.01%, $S_6^{(\Lambda)}(\tau)/S(\tau) \leq (1/6!)2^{-6} \simeq 2 \times 10^{-5}$ is already significantly smaller than the statistical error. Moments of order higher than the sixth are inaccessible unless the correlators with different τ values have strong correlations corresponding to the moments. One can obtain at most three statistically meaningful information on $\rho_\Lambda(\omega)$, *i.e.* $C_0^{(\Lambda)}$, $C_2^{(\Lambda)}$ and $C_4^{(\Lambda)}$, from the correlator. We emphasize that this limitation on the number of independent information on $\rho_\Lambda(\omega)$ is not resolved with the increase of N_τ .

When $\rho_{\text{high}}(\omega)$ gives rise to a large contribution to $S(\tau)$, the analysis of $\rho_\Lambda(\omega)$ should be much more difficult. This occurs particularly when $\rho(\omega)$ has a positive mass dimension, m , since $\rho(\omega)$ behaves as $\sim \omega^m$ for large ω for this case. Since the quark spectral function has a negative mass dimension, effects of $\rho_{\text{high}}(\omega)$ is expected to be small in our analysis.

While in the above argument we have limited our attention to the spectrum satisfying $\rho(\omega) = \zeta \rho(-\omega)$, one

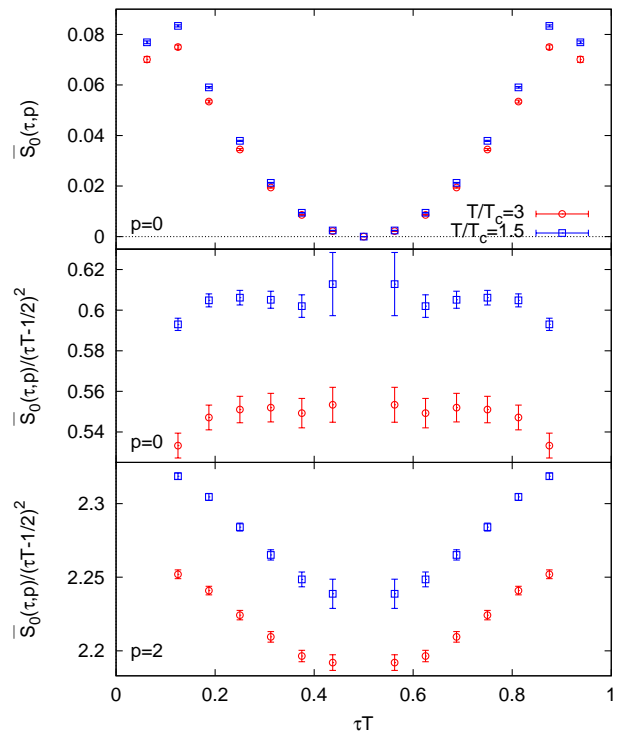


FIG. 7. Mid-point subtracted correlator $\bar{S}_0(\tau, 0)$ in the chiral limit (upper panel), and $\bar{S}_0(\tau, p)/(\tau T - 1/2)^2$ for $p = 0$ (middle) and $2(2\pi N_\tau/N_\sigma)T$ (lower).

can also derive a similar inequality for odd terms of $S_n^{(\Lambda)}(\tau)$ for general cases.

2. Quark correlator

Next, we inspect the structure of the quark correlator based on the discussion in the previous subsection. Let us first consider the correlator in the chiral limit with $p = 0$. In this case, the quark correlator takes non-zero values only in the temporal component of the vector channel, $S_0(\tau, 0)_{\text{lat}}$. The correlator in this channel is symmetric, $S_0(\tau, 0) = S_0(1/T - \tau, 0)$, and odd terms vanish in Eq. (A2). The values of C_n for even n are evaluated from the correlator as follows. First, the lowest moment, C_0 , is directly read off from the correlator at $\tau = 1/(2T)$; $C_0 = S_0(1/(2T), 0)_{\text{lat}}$. To examine higher order moments, we show in Fig. 7 the τ dependence of the mid-point subtracted correlator

$$\bar{S}_0(\tau, 0) \equiv S_0(\tau, 0) - S_0(1/2T, 0), \quad (\text{A8})$$

in the upper panel and that divided by $(\tau T - 1/2)^2$ in the middle panel. Using the latter plot, C_2 is estimated as $C_2 = \lim_{\tau T \rightarrow 1/2} \bar{S}_0(\tau, 0)/(\tau T - 1/2)^2$, while the deviation from the constant in this plot carries information of C_n for $n \geq 4$. The figure, however, shows

that $\bar{S}_0(\tau, 0)/(\tau T - 1/2)^2$ is constant within the statistical error except for the range of τ near the source, $|\tau T - 1/2| \gtrsim 0.3$, which receives the distortion effect and should be excluded from the analysis. This result shows that information on moments higher than four are buried in the statistical errors and inaccessible from our numerical results for this parameter.

This result is consistent with the argument in the previous subsection. As the pole ansatz predicts the poles of $\rho_0(\omega, 0)$ at $|\omega|/T \simeq 0.74$, spectral weight of $\rho_0(\omega, 0)$ is expected to concentrate more or less in the energy range $|\omega| < T$. Substituting $\Lambda = T$ to Eq. (A7), one obtains that $S_n^{(\Lambda)}(\tau, 0)_{\text{lat}}/S(\tau, 0)_{\text{lat}}$ are suppressed faster than $(2^n n!)^{-1}$. This upper limit is already the same order as the typical magnitude of the statistical error of the correlator, 10^{-3} , for $n = 4$. One thus can obtain only two statistically meaningful information on the quark spectrum, C_0 and C_2 , from the correlator for this parameter.

Since the quark correlator for $m_0 = p = 0$ contains only two information on the quark spectrum, any ansatz having more than two fitting parameters can well reproduce the correlator as long as it gives sufficiently small higher order moments. For example, we found that a fitting function with a single Gaussian peak for $\rho_0(\omega, 0)$ in the chiral limit,

$$\rho_0(\omega, 0) = \rho_+^M(\omega) = \frac{Z}{\sqrt{\pi}\Gamma} \exp\left(-\frac{\omega^2}{\Gamma^2}\right), \quad (\text{A9})$$

including two fitting parameters, Z and Γ , gives $\chi^2/\text{dof} \simeq 2.5$ for $T/T_c = 3$, which is less than twice larger than the one with the two-pole ansatz.

Evaluation of the quark spectrum for $m_0 = p = 0$ with the lattice correlator, therefore, is quite difficult. It, however, is notable that one can obtain some additional information on the spectrum for $m_0 = p = 0$ from the numerical analysis by using correlator for non-zero m_0 and p , because the spectral function is continuous with respect to these parameters. When m_0 (p) takes non-zero values, $\rho_+^M(\omega)$ ($\rho_+^P(\omega, p)$) is no longer an even function. Odd moments in Eq. (A2) then take non-zero values and these values provide additional constraints for the spectrum. At the same time the strength of $\rho_+^{M,P}$ shifts toward higher energies, as is expected from the free quark spectrum, $E = \sqrt{p^2 + m_0^2}$. The higher order

moments can then become larger, which makes the estimates of their values easier. To see this explicitly, in the lower panel of Fig. 7 we show $\bar{S}_0(\tau, p)_{\text{lat}}/(\tau T - 1/2)^2$ with $p = 2p_{\text{min}} = 2(2\pi N_\tau/N_\sigma)T$. The figure shows that this function clearly deviates from a constant, and hence contains statistically significant information on the fourth moment and higher. The number of information accessible with the quark correlator with this parameter thus is at least more than five. Since this number is larger than that of fitting parameters in the two-pole ansatz, the small χ^2/dof with the ansatz for this correlator is non-trivial. Since the simple two-poles ansatz Eq. (21) can reproduce the lattice correlator not only for $m_0 = p = 0$ but also over wide ranges of continuous parameters, it is expected that this ansatz reproduces at least a qualitative feature of the global structure of the quark spectrum in this parameter range, including $m_0 = p = 0$.

Similarly, one can argue that the single Gaussian ansatz, Eq. (A9), in the chiral limit and for $p = 0$ is most probably excluded as follows. The continuity of the quark spectrum means that if the Gaussian ansatz appropriately reproduces the structure of the spectrum, the ansatz has to be continuously connected to non-zero m_0 . We, however, have checked that several ansätze for $\rho_+^M(\omega)$ which reduce to Eq. (A9) at $m_0 = 0$ cannot give a reasonable chi-square with $m_0 \neq 0$; as far as we have checked, χ^2/dof obtained on all the ansätze grows rapidly as m_0 is increased. Although this analysis cannot completely exclude the form of Eq. (A9) in the chiral limit, it strongly suggests that the quark spectrum like Eq. (A9) is most probably ruled out even in the chiral limit.

ACKNOWLEDGMENTS

This work has been supported in part by a Grant-in-Aid for Scientific Research by Monbu-Kagakusyo of Japan (No. 21740182), the U.S. Department of Energy under contract DE-AC02-98CH10886. Numerical simulations have been performed on the BlueGene/L at the New York Center for Computational Sciences (NYCCS) which is supported by the U.S. Department of Energy and by the State of New York, and JUGENE at the John von Neumann Supercomputer Center (NIC) at FZ-Jülich, Germany, as well as the QCDOC computer of USQCD.

-
- [1] I. Arsene *et al.*, Nucl. Phys. A **757**, 1 (2005) [arXiv:nucl-ex/0410020]; B. B. Back *et al.*, *ibid.* **757**, 28 (2005) [arXiv:nucl-ex/0410022]; J. Adams *et al.*, *ibid.* **757**, 102 (2005) [arXiv:nucl-ex/0501009]; K. Adcox *et al.*, *ibid.* **757**, 184 (2005) [arXiv:nucl-ex/0410003].
- [2] M. Le Bellac, *Thermal Field Theory* (Cambridge University Press, Cambridge, England 1996).
- [3] R. J. Fries, B. Muller, C. Nonaka and S. A. Bass, Phys. Rev. C **68**, 044902 (2003) [arXiv:nucl-th/0306027].
- [4] R. V. Gavai and S. Gupta, Phys. Rev. D **73**, 014004 (2006) [arXiv:hep-lat/0510044]; S. Ejiri, F. Karsch and K. Redlich, Phys. Lett. B **633**, 275 (2006) [arXiv:hep-ph/0509051].
- [5] M. Cheng *et al.*, Phys. Rev. D **79**, 074505 (2009); C. Schmidt, Prog. Theor. Phys. Suppl. **186**, 563 (2010) [arXiv:1007.5164 [hep-lat]].
- [6] V.V. Klimov, Sov. J. Nucl. Phys. **33**, 934 (1981) [Yad. Fiz. **33**, 1734 (1981)]; H.A. Weldon, Phys. Rev. D **28**,

- 2007 (1983).
- [7] G. Baym, J. P. Blaizot and B. Svetitsky, Phys. Rev. D **46**, 4043 (1992).
- [8] M. Kitazawa, T. Kunihiro and Y. Nemoto, Phys. Lett. B **633**, 269 (2006) [arXiv:hep-ph/0510167]; Prog. Theor. Phys. **117**, 103 (2007) [arXiv:hep-ph/0609164].
- [9] M. Kitazawa, T. Kunihiro, K. Mitsutani and Y. Nemoto, Phys. Rev. D **77**, 045034 (2008) [arXiv:0710.5809 [hep-ph]].
- [10] M. Harada and Y. Nemoto, Phys. Rev. D **78**, 014004 (2008) [arXiv:0803.3257 [hep-ph]].
- [11] D. Muller, M. Buballa and J. Wambach, Phys. Rev. D **81**, 094022 (2010) [arXiv:1002.4252 [hep-ph]].
- [12] J. A. Mueller, C. S. Fischer and D. Nickel, Eur. Phys. J. C **70**, 1037 (2010) [arXiv:1009.3762 [hep-ph]].
- [13] S. -x. Qin, L. Chang, Y. -x. Liu and C. D. Roberts, Phys. Rev. D **84**, 014017 (2011) [arXiv:1010.4231 [nucl-th]].
- [14] D. Satow, Y. Hidaka and T. Kunihiro, Phys. Rev. D **83**, 045017 (2011) [arXiv:1011.6452 [hep-ph]].
- [15] H. Nakagawa, H. Yokota and K. Yoshida, Phys. Rev. D **85**, 031902 (2012) [arXiv:1111.0117 [hep-ph]].
- [16] Y. Hidaka, D. Satow and T. Kunihiro, Nucl. Phys. A **876**, 93 (2012) [arXiv:1111.5015 [hep-ph]].
- [17] F. Karsch and M. Kitazawa, Phys. Lett. B **658**, 45 (2007) [arXiv:0708.0299 [hep-lat]].
- [18] F. Karsch and M. Kitazawa, Phys. Rev. D **80**, 056001 (2009) [arXiv:0906.3941 [hep-lat]].
- [19] M. Hamada, H. Kouno, A. Nakamura, T. Saito and M. Yahiro, Phys. Rev. D **81**, 094506 (2010).
- [20] R. D. Pisarski, Phys. Rev. Lett. **63**, 1129 (1989); E. Braaten and R. D. Pisarski, Nucl. Phys. B **337**, 569 (1990); *ibid.*, **B339**, 310 (1990).
- [21] See, Appendix B in Ref. [18].
- [22] G. 't Hooft, Phys. Rev. D **14**, 3432 (1976) [Erratum-*ibid.* D **18**, 2199 (1978)].
- [23] C. Gatttringer, R. Hoffmann, S. Schaefer, Phys. Lett. **B535**, 358-362 (2002). [hep-lat/0203013].
- [24] T. Schafer, E. V. Shuryak, Rev. Mod. Phys. **70**, 323-426 (1998). [hep-ph/9610451].
- [25] O. Kaczmarek, F. Karsch, M. Kitazawa, W. Söldner, in progress.
- [26] H. T. Ding, A. Francis, O. Kaczmarek, F. Karsch, E. Laermann and W. Soeldner, Phys. Rev. D **83**, 034504 (2011) [arXiv:1012.4963 [hep-lat]]. [**ADD MORE?**]
- [27] A. Peshier and M. H. Thoma, Phys. Rev. Lett. **84**, 841 (2000) [arXiv:hep-ph/9907268].
- [28] G. Aarts and J. M. Martinez Resco, JHEP **0204**, 053 (2002) [arXiv:hep-ph/0203177].
- [29] P. Petreczky and D. Teaney, Phys. Rev. D **73**, 014508 (2006) [arXiv:hep-ph/0507318].
- [30] H. B. Meyer, Nucl. Phys. A **830**, 641C (2009) [arXiv:0907.4095 [hep-lat]].